Structural Basis for the Sequence-Specific DNA Strand Cleavage by the Enediyne Neocarzinostatin Chromophore. Structure of the Post-Activated Chromophore−DNA Complex†

Xiaolian Gao,*,‡ Adonis Stassinopoulos,§ Jeffrey S. Rice,‡ and Irving H. Goldberg*,§

Department of Chemistry, University of Houston, Houston, Texas 77204-5641, and Department of Biological Chemistry and Molecular Pharmacology, Harvard Medical School, Boston, Massachusetts 02115

Received September 19, 1994; Revised Manuscript Received November 1, 1994®

ABSTRACT: Neocarzinostatin chromophore (NCS chrom) belongs to a family of highly potent enediyne antitumor antibiotics which bind to specific DNA sequences and cause single- and/or double-strand lesions. NCS chrom−DNA complexes have eluded structural studies since the native form of the drug is extremely labile in aqueous conditions. We report the three-dimensional structure of the stable glutathione post-activated NCS chrom (NCSi-glu)−DNA complex [NCSi-glu-d(GGAGCGC)·d(GCGCTCC)] using NMR and distance geometry−molecular dynamics simulation methods. NCSi-glu interacts with the GCTC tetranucleotide on one strand and with the AGC trinucleotide on the other strand through the unique intercalation at the 5′-CT/5′-AG step and minor groove binding. The DNA−drug complex exhibits an extended, unwound V-shaped intercalation site and wider and shallower grooves than the free DNA duplex. The structure of the complex manifests specific van der Waals interactions and H-bond formation between the carbohydrate moiety and a specific DNA sugar/phosphate. Prominent among those are the contacts of the NCSi-glu residues with the functional groups in the minor groove that are characteristic of individual DNA bases. These results provide a structural model for understanding the sequence specificity of the single- and double-strand cleavage at the AGC and related sites by the enediyne NCS chrom.

Neocarzinostatin chromophore (NCS chrom,[1] Figure 1) exists in nature as a 1:1 complex with its host protein (Ishida et al., 1965; Napier et al., 1979; Kim et al., 1993). The isolated chromophore has been studied extensively as the prototype compound for a family of highly potent antitumor antibiotics [reviewed by Goldberg (1991)]. The target of action for these antibiotics, which include the chromophores of kedarcidin (Lam et al., 1991) and C-1027 (Otani et al., 1988) proteins, as well as the enediyne compounds dynemicin (Konishi et al., 1990), calicheamicins, and esperamicins (Lee et al., 1987; Golik et al., 1987), is thought to be cellular DNA [reviewed by Dedon and Goldberg (1992)]. The novelty of these molecules stems from their chemical structure which consists of a highly strained enediyne ring and a variety of substituent groups (Edo et al., 1985; Nicolaou & Dai, 1991). For NCS chrom, nucleophilic addition of thiol to the C12 position is required for promoting DNA cleavage *in vitro* and *in vivo*. In NCS chrom, activation of the enediyne ring results in the formation of a cumulene intermediate, which spontaneously rearranges to give a transient 2,6-biradical species (Figure 1) (Myers, 1987). When NCS chrom is bound to double-stranded DNA, the subsequent hydrogen abstraction from deoxyribose sugars

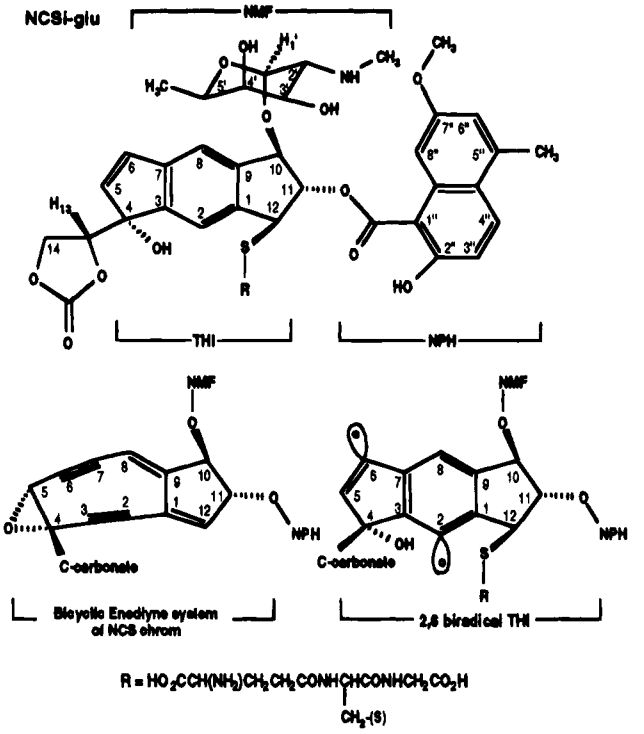

FIGURE 1: Chemical structure of NCSi-glu (upper drawing), NCS chrom (lower left drawing), and the 2,6-biradical species (lower right drawing). The abbreviations for substituents are NMF (2-*N*-methylfucosamine), THI (tetrahydroindecene), and NPH (naphthoate).

† This research is in part supported by grants from the American Cancer Society to X.G. (JFRA-493) and from the NIH to I.H.G. (CA44257).

* To whom correspondence should be addressed.

‡ University of Houston.

§ Harvard Medical School.

® Abstract published in *Advance ACS Abstracts,* December 15, 1994.

[1] Abbreviations: 1D, one dimensional; 2D, two dimensional; COSY, 2D *J*-coupling correlation spectroscopy; DG, distance geometry; DQF, double-quantum filtered; MD, restrained molecular dynamics; NMR, nuclear magnetic resonance; NCS chrom, neocarzinostatin chromophore; NCSi-glu, glutathione postactivated NCS chrom; NMF, 2-*N*-methylfucosamine; NOE, nuclear Overhauser effect; NOESY, 2D NOE spectroscopy; NPH, naphthoate; THI, tetrahydroindacene; TOCSY, 2D total correlated spectroscopy.

0006-2960/95/0434-40$09.00/0 © 1995 American Chemical Society

ultimately causes single-strand lesions (ss) with base specificity (T > A ≫ C > G) and double-strand (ds) lesions with sequence specificity (Goldberg, 1991). The ds lesions are lethal due to inefficient repairing of the strand breaks and, thus, are connected with the cytotoxicity and mutagenicity of the NCS chrom. Recently, an alternative mechanism of drug activation *via* intramolecular nucleophilic attack by the C1″ enolate anion of NPH on C12 has been found to generate a site-specific break selectively at a DNA bulge (Kappen & Goldberg, 1993; Hensens et al., 1994).

The major sites of ss damage for ds DNA are T residues with H5′ or H4′ abstraction. Ds damage occurs mainly at AGC·GCT- and AGT·ACT-containing sequences (Goldberg, 1991; Dedon et al., 1992). At the AGC·GCT sequences H1′ abstraction at the C residue generates an abasic site on one strand. This is accompanied by H5′ abstraction at the T residue, which generates a strand break on the opposite strand. The observed sequence specificity of NCS chrom indicates that the cleavage is preceded by binding. Classical biophysical studies have shown that NCS chrom binds to DNA through intercalation of the naphthoate moiety (Povirk & Goldberg, 1980; Povirk et al., 1981) and provided evidence for minor groove binding (Dasgupta & Goldberg, 1985). Structural models of the complexes, involving postactivated NCS chrom analogs and a DNA duplex 5′-GAGCG·CGCTC-3′, have been proposed on the basis of molecular mechanics and molecular dynamics calculations (Galat & Goldberg, 1990). A major binding mode revealed in that study involved intercalation of NPH into the CT/AG step with the tetrahydroindacene (THI) ring aligned in the minor groove in such an orientation that C6 of the NCS chrom analog is close to the T(C5′) of one strand and C2 of the NCS chrom analog is close to the C(C1′) of the opposite strand. On the basis of this system, other revised post-activated NCS chrom−DNA models were presented (Sugiyama et al., 1992; Elbaum & Schreiber, 1994). Strong support for the model has come from studies showing that deuterium atoms from T(C5′) and C(C1′) are abstracted by C6 and C2 of the NCS chrom, respectively (Meschwitz & Goldberg, 1991; Meschwitz et al., 1992). However, although NMR studies of the nonintercalating enediyne calicheamicin γ_I−DNA complexes have appeared (Walker et al., 1993; Langley et al., 1994); Paloma et al., 1994), no NMR or X-ray structural data for any of the NCS chrom−DNA complexes have been reported.

In this report, we describe the three-dimensional structure of a complex that contains the glutathione post-activated NCS chrom (NCSi-glu, Figure 1) binding to the AGC·GCT trinucleotide site in the 5′-d($G_1G_2A_3G_4C_5G_6C_7$)·d($G_8C_9G_{10}C_{11}T_{12}C_{13}C_{14}$)-3′ duplex. NCSi-glu closely resembles the reactive 2,6-biradical (Figure 1), which is the hydrogen abstraction species, and, unlike the extremely labile native chromophore, is stable under the conditions used for NMR studies. NCSi-glu and the native NCS chrom have the same substituents; amino sugar, naphthoate, and cyclocarbonate groups (Figure 1).

MATERIALS AND METHODS

Formation of the NCSi-glu−DNA Complex. The two heptanucleotide strands were chemically synthesized and purified by reverse-phase HPLC as described previously (Gao & Jones, 1987). The annealing of the two strands at room temperature was monitored by one-dimensional (1D) proton NMR recorded in D_2O. NCSi-glu was synthesized and purified as reported (Chin & Goldberg, 1993). The compound dissolved in methanol is stable at 10 °C for an extended period of time. The NCSi-glu−DNA complex was generated at 15 °C by gradual addition of the DNA duplex dissolved in 5 mM PO_4^{3-} and 0.1 mM EDTA (all salts used for NMR samples are in sodium form unless otherwise indicated) to a sample of NCSi-glu dissolved in methanol-d_4. Complex formation was judged from the disappearance of sharp signals of the free NCSi-glu in 1D ^1H NMR spectra. The resulting samples were lyophilized and redissolved in H_2O for observation of imino protons. The shifted imino proton resonances provided additional evidence for complex formation. Two samples were generated for NMR studies. Sample I contains 50% 1:1 NCSi-glu−DNA complex and 50% free duplex, and complete complex formation yielded sample II, which has a concentration of ~0.3 mM in 5 mM PO_4^{3-} and 0.1 mM EDTA, pH 5.5−5.8 (spectra were invariant in the pH range of 5.5−7.0).

NMR Experiment. NMR experiments were performed on spectrometers of 600 MHz at the University of Houston and 750 MHz at Bruker Analytische Messtechnik GMBH (Germany).

(a) The Free Duplex and the Free NCSi-glu. A set of two-dimensional (2D) NOESY and various COSY data were collected and analyzed for the free duplex at 15 °C (~2 mM in an aqueous solution containing 5 mM sodium phosphate and 0.1 mM EDTA, pH 5.8). The strong H_2O signal was suppressed using the jump−return pulse sequence (Planteau & Guéron, 1982) in 1D and 2D experiments. A similar set of 2D data was obtained for the free NCSi-glu at 10 °C (in methanol-d_4/D_2O).

(b) The NCSi-glu−DNA Complex. 2D exchange spectra were recorded in D_2O (250-ms mixing time) and H_2O (200-ms mixing time) for the sample containing a mixture of the complex and the free duplex (sample I). 2D $^1H-^{31}P$ COSY, ^1H DQF-COSY, TOCSY (100 and 150 ms), and NOESY (70, 100, 150, and 250 ms) were recorded in D_2O and H_2O in the 5−20 °C temperature range for sample II. Digital resolution of 2−4 Hz was used for various data sets. Sweep widths of 2000 Hz (3.33 ppm) in the proton dimension and 1200 Hz (4.55 ppm) in the ^{31}P dimension were used to acquire the $^1H-^{31}P$ COSY spectrum with a digital resolution of 1.95 Hz in F_2 and 4.7 Hz in F_1 (after data processing), respectively. ^1H chemical shifts (Table 1, uncorrected for solvent D_2O or H_2O) were referenced to the HOD resonance of 4.70 ppm at 25 °C. ^{31}P resonances were referenced to external trimethyl phosphate in an aqueous solution containing 0.1 M NaCl (pH 6.5).

NMR data were processed using the FELIX 2.3 program (Biosym Technologies, Inc.) on an INDIGO/ELAN workstation. NOESY data were apodized by a 90° phase-shifted sine-bell function; DQF-COSY and TOCSY data were multiplied by a 30° phase-shifted skewed sine-bell function and an unshifted sine-bell function was applied to the COSY-35 data prior to Fourier transformation. Cross-peak and volume files were obtained from the database available from the FELIX program.

NMR Restraints. The cross peaks of the 150-ms NOESY spectrum recorded at 750-MHz proton frequency were assigned by a semiautomated procedure, which considers all possible assignments for each cross peak in the spectrum

(Gao & Burkhart, 1992). These possibilities were analyzed, and the confirmed assignments were converted to distance restraints using the two-spin approximation. The upper and lower distance bounds initially were at 50% of the equilibrium distances. The maximum interproton distance was generally limited to 5.0 and 5.5 Å for non-methyl and methyl protons, respectively. The minimum interproton distance limit was set to 1.8 Å. Distance and sugar conformation restraints were supplemented by the information abstracted from various 600-MHz 2D data sets, such as the spectra recorded in H_2O for Watson−Crick base-pairing hydrogen bonds and NOESY of 100- and 250-ms mixing times for nonexchangeable protons. A detailed description of NMR distance and dihedral angle restraints is given in Tables 2 and 3. The glutathionyl side chain (except for the Cys residue) was not included in the calculation due to the lack of proton assignments in this portion of the molecule.

Structure Calculation. Distance geometry (DG) and restrained molecular dynamics (MD) simulations were used to generate a family of structures using the XPLOR program [Molecular Simulations Inc. (MSI)] following procedures similar to what is described in the literature (Kuszewski et al., 1992). The NCSi-glu parameter file was generated from the Quanta program (MSI). NOE restraints in the form of square-well potential and a van der Waals nonbonded repulsion function were used in the initial DG embedding. Typical DG calculation steps involved partial metrization (using subsets phosphorus, C3′, C5′, C1′, N9, N1, C2, C4, N3, and all atoms in NCSi-glu), embedding, regularization, and refinement. The DG structures were further refined using MD simulations which employ NMR-based distance and dihedral target functions in addition to the standard potential energy terms. The general MD procedures involved first heating the molecule to 700−1000 K in steps of 20−30° while increasing the force constants of NOE restraints to target values, which varies from 10 to 40 kcal/mol depending on the type definition of NOEs (Table 3). The ceiling factor was set at 500 kcal/(mol Å^2). The system was then gradually cooled and equilibrated for an additional 1−2 ps followed by an energy minimization. After each calculation, distance and dihedral angle violations, geometry, and energies of the calculated structures were evaluated. The discrepancy between calculated structures and experimental inputs was further minimized by varying temperature gradient and time steps in refinement protocols. Some ambiguities present in the NMR data can be resolved by distance comparison with the calculated structures, and thus, improved restraint files were used in subsequent calculations. This procedure was repeated until satisfactory results were obtained (Table 3).

The structure of the DNA duplex in the complex was characterized using the CURVE program V4.1 (Lavery & Sklenar, 1988). Structure statistics was presented as mean values ± root mean standard deviations (rmsd) derived from the five calculated structures and as averaged values measured from the averaged and energy-minimized structure.

RESULTS AND DISCUSSION

Preliminary studies of complex formation were conducted to ensure the selected sequence contains a native binding site. Indeed in the presence of glutathione, NCS chrom generates a single ds lesion at the AG<u>C</u>•G<u>C</u><u>T</u>• site (Stassinopoulos and Goldberg, unpublished results). Cleavage was directly observed at the <u>T</u> site, while a subsequent base treatment was necessary for the expression of damage at the <u>C</u> site, in agreement with the reported abasic site formation in other longer oligonucleotide sequences (Kappen et al., 1988) and restriction fragments (Povirk & Goldberg, 1985). Additional evidence of the complex formation was the quenching of fluorescence (Goldberg, 1991) upon incubation of NCSi-glu with increasing amounts of the duplex in Tris-HCl, pH 7, and 10% MeOH, indicating intercalative binding of NCSi-glu to target DNA. Standard Scatchard analysis gave a DNA dissociation constant of ~16 μM for NCSi-glu in 10% MeOH−aqueous solution. Similar binding studies with NCS chrom were unsuccessful because of its rapid decomposition even at pH 5. However, affinity cleavage experiments gave a dissociation constant of 4 μM for NCS chrom to the AGC site, suggesting tighter binding compared to that of NCSi-glu.

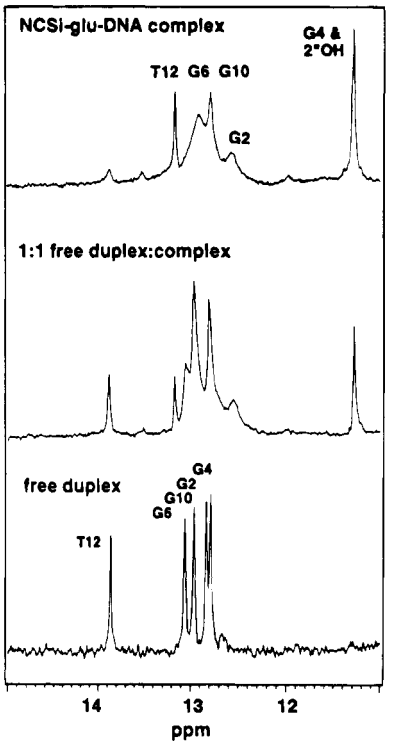

FIGURE 2: 1D plots of the imino proton spectral region of the free duplex at 12 °C (bottom), sample I at 12 °C (50% free duplex and 50% NCSi-glu−DNA complex) (middle), and sample II at 11 °C (the NCSi-glu−DNA complex, one drug molecule per duplex) (top).

NMR Spectral Analysis. Five imino protons were observed in the free duplex and in the complex (Figure 2), while the two terminal imino protons were not observed in these spectra due to end-fraying. Inspection of 1D spectra shown in Figure 2 indicates the formation of predominantly one complex, signified by the large upfield shifts in the complex of the hydrogen-bonded imino protons of T12 and G4 by 0.71 and 1.48 ppm, respectively (Table S1). An expanded NOESY spectrum recorded in H_2O for sample I is shown in Figure 3. T12 and G4 imino proton resonances were conveniently assigned in the complex through exchange cross peaks. Thus, the three sharp imino proton resonances in the complex (top spectrum, Figure 2) were assigned to G4, G10, and T12 residues at the AGC•GCT binding site (Figure 5). The remaining two broad imino resonances were assigned to G2 and G6 imino proton resonances, respectively. T12 imino proton and NCSi-glu(2″OH) resonances at 11.31 and

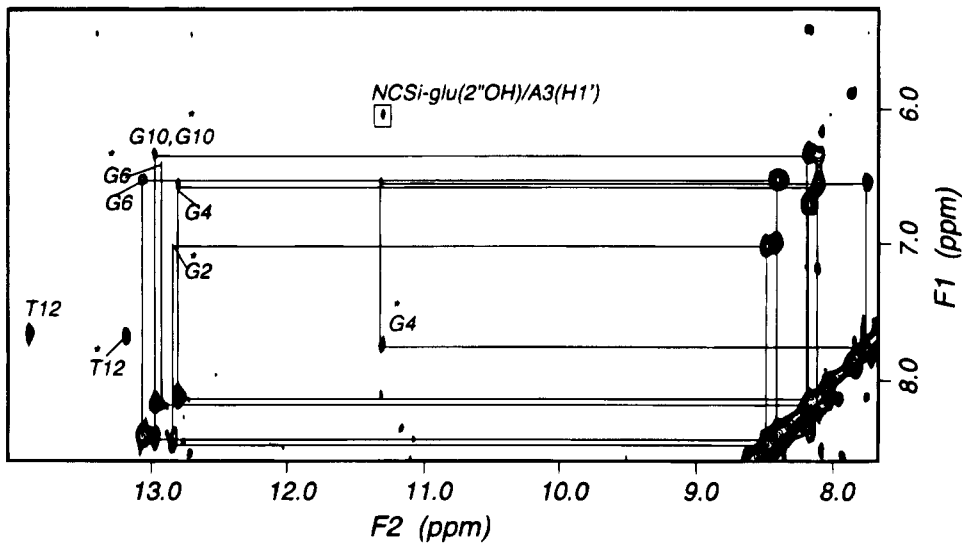

FIGURE 3: Expanded exchange spectrum (200-ms mixing time) of sample I (50% free duplex and 50% NCSi-glu−DNA complex). The spectrum was recorded in H_2O at 5 °C. The F_2 axis covers resonances of G imino and C hydrogen-bonded amino protons, and F_1 covers hydrogen-bonded and nonbonded amino protons of C residues.

11.29 ppm were resolved in 2D NOESY spectra recorded in H_2O. The formation of the complex stabilizes the duplex at the binding site, since the line widths of the imino proton resonances of the central 5′-AGC•GCT-3′ sequence in the complex remained sharp, while those in the free duplex were significantly broadened at 27 °C (data not shown).

NMR spectra of nonexchangeable proton resonances were analyzed by a combined use of three types of connectivities: through-bond connectivities (DQF-COSY), through-multiple bond connectivities (TOCSY), and through-space connectivities (NOESY) (Wuthrich, 1986). ^{1}H connectivity and cross-peak assignments have been completed for both the free duplex (Table S1) and NCSi-glu. Detailed NMR analyses and comparisons of the free duplex and free NCSi-glu and their complexes will be published separately elsewhere. These results suggest formation of a canonical right-handed helix for the free duplex. The chemical shifts of the ^{1}H and ^{31}P resonances of the free duplex and NCSi-glu provide markers for complex formation and conformational studies of the complex.

Chemical shift assignments of the complex were obtained from a combined analysis of various data sets. NOE cross-peak assignments were primarily based on the NOESY recorded on the 750-MHz NMR instrument, which exhibits superior signal to noise ratio compared to the 600-MHz data. As a comparison, the spectra of an expanded region (H1′ in F_2 and H2′,2″ in F_1) recorded on the two spectrometers under similar conditions are shown in Figure 4. This figure illustrates the good spectral quality and well-resolved cross peaks for the complex achieved on the higher field instrument with limited sample concentration. The 2D exchange spectra of sample I were very informative in providing lead assignments in the complex, which were obtained by the analysis of exchange cross peaks between resonances known in the free duplex and resonances in the complex. The majority of the DNA proton resonances including sugar H3′ (except for the G10 residue) and H4′ (except for the G6, C9, and G10 residues) were identified by following intra- and interresidue connectivities (Table 1) (Wuthrich, 1986). ^{31}P resonances of key residues at the binding site (A3−G4, C11−T12, T12−C13) have been assigned (Table 1). ^{1}H

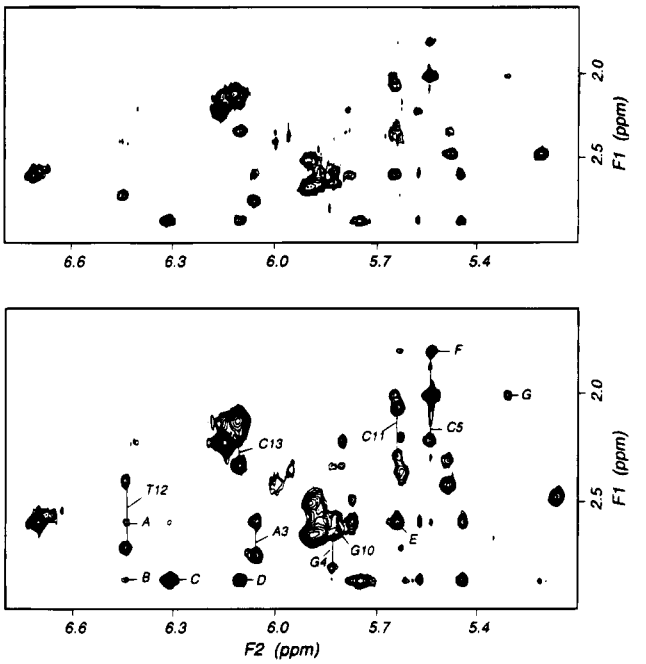

FIGURE 4: Expanded NOESY (150 ms, 3 °C) plots of the NCSi-glu−DNA complex in the spectral region of 5.1−6.8 ppm (F_2) and 1.6−3.0 ppm (F_1). The comparison of the data sets recorded at 600 MHz shown in (A, top) and at 750 MHz shown in (B, bottom) illustrates significant enhancement in the signal to noise ratio and good spectral quality achieved on the higher field instrument. The assignments of H1′−H2′ and H1′−H2″ NOEs related to the residues A3, G4, C5, G10, C11, T12, and C13 at the binding site are indicated in (B). These NOEs are well resolved. NOE cross peaks A−G in spectrum B are from intermolecular proton−proton contacts: A, T12(H1′)−NPH(H7″M); B, T12(H1′)−NMF(H2M); C, A3(H1′)−NMF(H2M); D, C13(H1′)−NMF(H2M); E, C11-(H1′)−NPH(H7M); F, T12(H5M)−NPH(H6″); G, C11(H5)−NPH-(H5″M).

assignments have been obtained for all NCSi-glu resonances except for those of the glutathionyl side chain (Table 1). Chemical shift comparison of the complex (DNA proton resonances) with the free duplex indicates the most shifted resonances belong to G4, C11, and T12 residues (Table S1). For instance, the resonances of base H6 and methyl, H1′, H2′, H2″, and H4′ of T12 are downfield shifted by 0.24,

Table 1: ^{1}H and ^{31}P Chemical Shifts of the NCSi-glu−DNA Complex[a]

	HN	NH_2(b)	NH_2(nb)	H8	H2	H6	H5	H1′	H2′	H2″	H3′	H4′	H5′,H5″	^{31}P
G1				7.70				5.48	2.31	2.43	4.69	4.04	3.57, 3.57	−3.82
G2	12.60			7.67				5.16	2.48	2.48	4.86	4.20	3.99, 3.99	−3.69
A3				8.04	7.68			6.05	2.60	2.75	5.02	4.33	4.04, 4.12	−2.04
G4	11.31			7.72				5.83	2.34	2.81	4.67	4.42	4.01, 4.29	
C5		8.18	6.70					5.54	1.87	2.22	4.73	4.05	4.05, 4.05	
G6	13.07			7.75				5.77	2.49	2.60	4.89			−3.57
C7						7.56	5.63	6.11	2.13	2.13	4.44	4.00		
G8				7.86				5.89	2.51	2.66	4.75	4.15	3.64, 3.64	
C9		8.09	6.33			7.39	5.31	5.63	2.20	2.36	4.75			
G10	12.79			7.81				5.82	2.59	2.64				
C11		7.75	6.54			7.38	5.31	5.64	2.29	2.07	4.90[b]	4.12		−3.33
T12	13.18					7.66	1.81	6.44	2.41	2.72	4.99	4.53	4.09, 4.25	−3.56
C13		8.41	6.97			7.56	5.63	6.11	2.20	2.34	4.88	4.27	4.10	
C14						7.68	5.81	6.14	2.23	2.23	4.50	4.25	4.01, 4.10	
NCSi-glu														
NPH	2″OH	H3″	H4″	HNM	H6″	H7M	H8″							
	11.29	5.65	7.28	2.01	5.54	2.60	6.70							
NMF	H1′	H2′	H2M	H3′	H4′	H5′	HFM							
	6.31	3.19	2.87	3.76	3.45	3.15	0.96							
THI	H2	H5	H6	H8	H10	H11	H12	H13	H14*					
	7.51	6.39	6.89	7.65	5.44	5.57	4.85	5.07	4.50					
CYS	HA	HB1	HB2											
	4.58	2.60	3.04											

[a] Chemical shift assignments of nonexchangeable resonances were obtained from the 150-ms NOESY recorded at 5 °C. The sample solution contained 5 mM PO_4^{3-}; the pH was 5.5. Exchangeable proton assignments were obtained from a mixture of 1:1 complex−duplex at 5 °C. The sample contained 5 mM PO_4^{3-} 20 mM NaCl; the pH was 5.5. [b] Assigned from the $^{1}H-^{31}P$ COSY spectrum for unresolved methylene H.

Table 2: Intermolecular Distances (Å) in the NCSi-glu−DNA Complex[a]

		DNA residue									
NCSi-glu		A3		G4		C11		T12		C13	
NPH	H2OH	H1′	2.8[b] (3.2 ± 0.1)[c]								
		H2′	3.0 (3.5 ± 0.0)								
		H2″	3.0 (2.4 ± 0.0)								
	H3″	H8	3.6 (4.0 ± 0.1)								
	HNM					H5	3.1 (4.5 ± 0.1)				
	H6″					H6	3.4 (3.6 ± 0.1)	M5	2.8 (3.2 ± 0.1)		
						H2′	4.3 (4.3 ± 0.1)				
						H2″	4.2 (4.1 ± 0.1)				
	H7M					H1′	2.4 (2.7 ± 0.0)	H6	2.7 (3.4 ± 0.0)		
						H2′	4.5 (4.6 ± 0.0)	M5	3.5 (4.2 ± 0.0)		
						H2″	3.7 (3.2 ± 0.0)	H1′	3.4 (4.4 ± 0.0)		
								H4′	3.7 (4.9 ± 0.1)		
NMF	H1′	H2	4.0 (3.8 ± 0.0)								
	H2′							H1′	3.9 (4.9 ± 0.0)	H4′	2.7 (2.5 ± 0.0)
										H5′	2.7 (4.7 ± 0.0)
	H2M	H2	2.4 (3.3 ± 0.0)	H1′	3.6 (6.9 ± 0.1)[d]			H1′	3.4 (5.2 ± 0.0)	H1′	2.6 (3.2 ± 0.0)
	HFM							H1′	3.9 (5.1 ± 0.0)	H4′	3.3 (3.6 ± 0.0)
								H4′	2.9 (4.4 ± 0.0)	H5′	2.7 (3.8 ± 0.0)
THI	H6							H4′	2.8 (2.1 ± 0.0)		
								H5′	3.0 (2.9 ± 0.0)		
								H5″	3.3 (3.7 ± 0.0)		
	H8							H1′	2.7 (2.6 ± 0.0)		
								H4′	3.0 (2.8 ± 0.0)		
								H5′[e]	3.6 (4.2 ± 0.0)		
	H10	H2	3.0 (3.8 ± 0.1)					H1′	3.4 (3.4 ± 0.0)		
	H11	H2	4.7 (5.0 ± 0.1)								
	H12			H1′	3.2 (3.7 ± 0.1)						

[a] NOEs of nonexchangeable protons were assigned from a 150-ms NOESY spectrum recorded at 5 °C. [b] Equilibrium distances used in DG and MD calculations. Lower and upper bounds vary from 0.05 to 3 Å depending on the type of protons, intensity, resolution, and quality of NOE peaks. [c] Distance mean values and deviations from the five final structures. [d] NOEs are very weak, and the upper distance limit was 6.6 Å. [e] H5* is the pseudoatom for H5′ and H5″ protons.

0.26, 0.44, 0.28, 0.26, and 0.41 ppm, respectively (Table S1). The ^{31}P resonance of the A3−G4 phosphate linkage resonates at −2.04 ppm, reflecting a 2.05 ppm downfield shift upon complex formation (Table S1). These shifted resonances support the structure of the complex discussed later in this paper.

The spectral features of the complex are consistent with a right-handed helix in which each residue adopts an anti-glycosidic conformation. Sugar H2′ and H2″ protons of the C11 residue exhibited "inverted" chemical shifts (H2′ is downfield shifted compared to that of H2″) (Table 1). Sequential NOE connectivities were interrupted at the A3−

Table 3: Summary of Structural Calculation Results[a]

statistical results	⟨SA⟩	$\overline{(SA)}$r
molecular geometry deviation from ideal values		
bond length[b] (577) (Å)	0.00041 ± 0.00003	0.00042
bond angle (1040) (deg)	3.297 ± 0.014	3.726
chirality and planetary ring (287) (improper angles, deg)	3.397 ± 0.083	3.370
rms deviations of coordinates (Å)	pairwise	⟨SA⟩/$\overline{(SA)}$r
all atoms	0.766 ± 0.134	0.534 ± 0.102
residues 3−5, 10−13, and NCSi-glu	0.615 ± 0.049	0.461 ± 0.081
rms deviation from experimental restraints		
dihedral angles (13) (deg)	6.179 ± 0.389	2.499
NOE (Å)		
NCSi-glu and DNA (38)	0.098 ± 0.009	0.076
H-bond (20)	0.094 ± 0.002	0.057
intra-NCSi-glu (27)	0.101 ± 0.007	0.113
intra-DNA (168)	0.048 ± 0.002	0.033

[a] SA are the final five DG/MD structures and ⟨SA⟩ is the ensemble of SA; $\overline{(SA)}$r is the structure obtained by averaging the Cartesian coordinates of SA followed by energy minimization. The nonterminal DNA sugars were restrained in the range of C2′-endo (dihedral angles of C5′−C4′−C3′−O3′ = 125 ± 15°; for C5 the angle is 125 ± 35°). NMF was restrained in a chair conformation as observed by NMR. No violation of dihedral angles is larger than 15°. Distance restraints (excluding fixed distances) were divided into four classes, to which were assigned different force constants and distance bounds depending on the quality and importance of the cross peaks. These NOE types are NCSi-glu and DNA, intermolecular distances between NCSi-glu and the DNA duplex; H-bond, Watson−Crick H-bonds; intra-NCSi-glu and intra-DNA, intraresidue distances of NCSi-glu and the DNA duplex, respectively. The intermolecular proton distances between NCSi-glu and DNA include those well-defined and unambiguously assigned and, therefore, were heavily weighted and given relatively tight bounds. Weaker force constants (10−20 vs 40 kcal/mol) were used for distances related to the nonbinding region of DNA to account for the uncertainty in data due to additional flexibility observed in that portion of the complex (described in the Results and Discussion section). No distance violation is larger than 0.3 Å except for one violation of 0.46 Å for the distance between the *N*-methyl of NCSi-glu and G4(H1′) protons in one of the five structures. [b] The shake algorithm was applied to all atoms in MD calculations.

G4 and C11−T12 steps. This, in conjunction with several intermolecular aromatic proton−proton contacts, indicates the intercalative binding between the A3•T12 and G4•C11 residues. Table 2 summarizes the NOEs observed between NCSi-glu and the duplex. Many contacts involving NCSi-glu and DNA adenine H2 and sugar H1′ protons unambiguously position the NCSi-glu in the minor groove adjacent to the AGC site. NOESY spectral assignments led to the identification of a total of 233 interproton interactions, including as many as 65 NOEs related to NCSi-glu (27 intra- and 38 intermolecular correlations; Table 2). The analysis of various COSY spectra provided qualitative information on couplings of H1′−H2′,H2″ and H3′−H4′ for the DNA sugars and H2′−H3′ for the NMF of NCSi-glu. Generally, DNA H1′−H2′ couplings for the nonterminal sugars are stronger than those of the H1′−H2″, and only H3′−H2′ coupling cross peaks are detected in the corresponding spectral region. These results suggest that the conformations of DNA sugar residues are in the C2′ family (Table 3). NMR data showed some dynamic features at the nonbinding region 3′ to C5•G10 (C5−G6 and C9−G10), while the other end of the nonbinding region is well-defined. This was reflected in the line broadening of the G6 proton resonances and C9 nonexchangeable proton resonances and in the breakdown of sequential NOE connectivities at C5−G6 and C9−G10 steps.

Structure Refinement. The NMR results were incorporated as initial distance and dihedral angle restraints in structure calculations as detailed in the legend of Table 3. The unambiguously assigned intermolecular NOEs between NCSi-glu and the duplex (Table 2) are critical for defining the conformation of the complex. These NOEs were tightly restrained in the calculation. On the other hand, terminal residues were flexible, and thus, larger interproton distance bounds and less weight were applied to the related NOEs in the calculation. The structure computation was carried out in an iterative manner in which distances derived from the calculated structures were compared with experimental data. On the basis of these analyses, distance bounds and NOE force constants of various groups of NOE restraints were adjusted, and a new generation of structures was calculated using newly modified protocol. The final structures were selected or rejected on the basis of several criteria, such as the number and the pattern of distance and dihedral violations, chirality and nonplanar violations, and the total energy of the molecule. Five structures and an energy-minimized average structure are presented as the final results in Figure 5. These converged structures show good bond and angle geometry (Table 3) and in general satisfy NMR-derived distances and dihedral angles. The NCSi-glu binding site (A3G4C5•G10C11T12C13) is especially well-defined as shown by the reduced Cartesian coordinate rms deviations and narrower distribution of these values compared to those measured from total structures (Table 3).

Table 4: Rotatable Bonds of NCSi-glu in the Complex[a]

dihedral angle	mean value (deg) of ⟨SA⟩	deviation	value (deg) from averaged ⟨SA⟩
(C3) (C4) (C13) (C14)	−70.68	0.80	−71.43
(C11) (C12) (S) (CB)	−70.36	0.99	−70.39
(C11) (C10) (O1′) (C1′)	147.16	0.60	147.90
(C10) (O1′) (C1′) (C2′)	−150.43	0.48	−147.66
(C1′) (C2′) (NHMe) (CNMe)	41.47	2.25	33.18
(C12) (C11) (O) (C=O)	−169.02	0.62	−166.12
(C11) (O) (C=O) (C1″)	172.49	0.47	172.10
(O) (C=O) (C1″) (C2″)	−120.96	1.12	−124.38
(C6″) (C7″) (O7″Me) (CO7″Me)	169.77	2.16	175.54

[a] See Table 3 for definitions of ⟨SA⟩ and the averaged ⟨SA⟩.

Overall Structure of the Complex. As shown in Figure 5, NCSi-glu adopts an extended form in the complex, interacting with the G10C11T12C13 tetranucleotide on one strand and with the A3G4C5 trinucleotide on the other strand. The geometry parameters related to the rotatable bonds of NCSi-

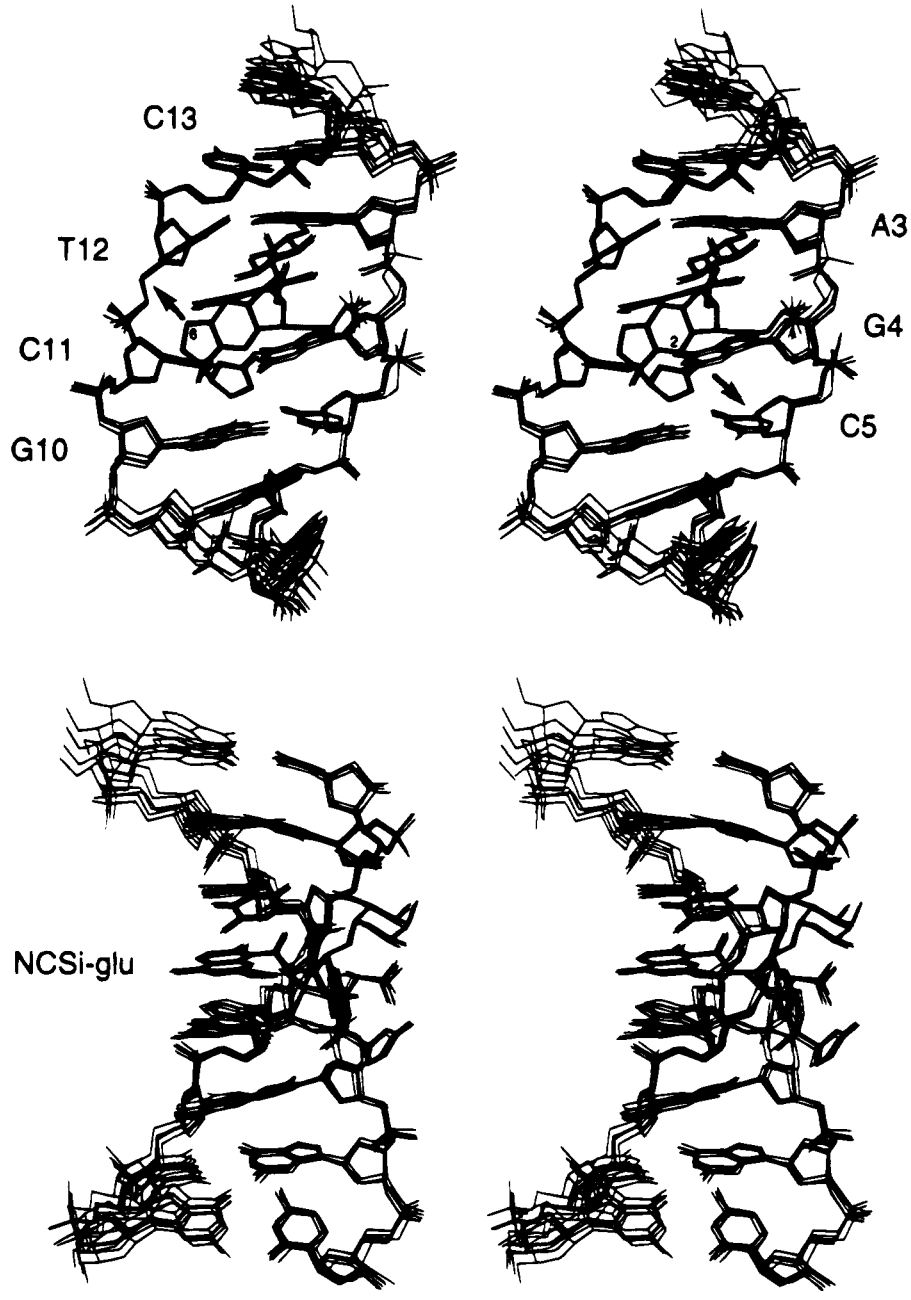

FIGURE 5: Overlay stereoview (cross-eyed) of five calculated structures and the energy-minimized average structure of the NCSi-glu–d(GGAGCGC)•(GCGCTCC) complex. (A, top) A view into the minor groove, displaying the extended, V-shaped binding site. The C5(1′) and T12(5′) cleavage sites by the C2 and C6 radicals, respectively, are indicated. (B, bottom) A view displaying the intercalation binding mode and the opening of both the major and minor grooves (left and right side of the drawing, respectively).

glu are listed in Table 4. These results show that the NPH ring is directed away from the enediyne ring and projects into the helix between the A3•T12 and G4•C11 base pairs, confirming previous modeling studies (Galat & Goldberg, 1990; Sugiyama et al., 1992; Elbaum & Schreiber, 1994), while the NMF, THI, and the cyclocarbonate substituent groups contribute to the minor groove binding. The orientation of the NMF sugar relative to the postactivated enediyne core (THI) is determined by the two glycosidic bonds, which were found in the anti-conformation range (Table 4). An opposite orientation for the carbohydrate unit was predicted by the modeling studies (Galat & Goldberg, 1988; Hawley et al., 1989; Sugiyama et al., 1992). In the absence of experimental data, that sugar orientation may be derived from the crystal structure of the monoaminocarbohydrate anthracycline daunomycin–DNA complex (Quigley et al., 1980). The carbonyl group of the cyclocarbonate moiety is exposed to solvent with the methine and methylene protons facing toward the minor groove.

The complex is stabilized by the stacking interactions through intercalation (Figure 6A, Table 2) and by the backbone helical (Figure 6B) and minor groove contacts (Figure 6C) through van der Waals interactions. Specifically, as shown in Figure 6A, one of the two NPH six-membered rings (the one containing C1″) stacks on the purine ring of G4, while the A3 and C11 bases are partially stacked on the NPH ring. These alignments are supported by the large upfield-shifted resonances of NPH ring protons, such as H3″ (1.17 ppm), 7″-methyl (0.98 ppm), and H8″ (1.61 ppm), and duplex imino protons of the G4 and T12 residues in the complex compared to those of the free NCSi-glu or the free duplex (Table S1, *vide supra*). The intercalation of NPH of

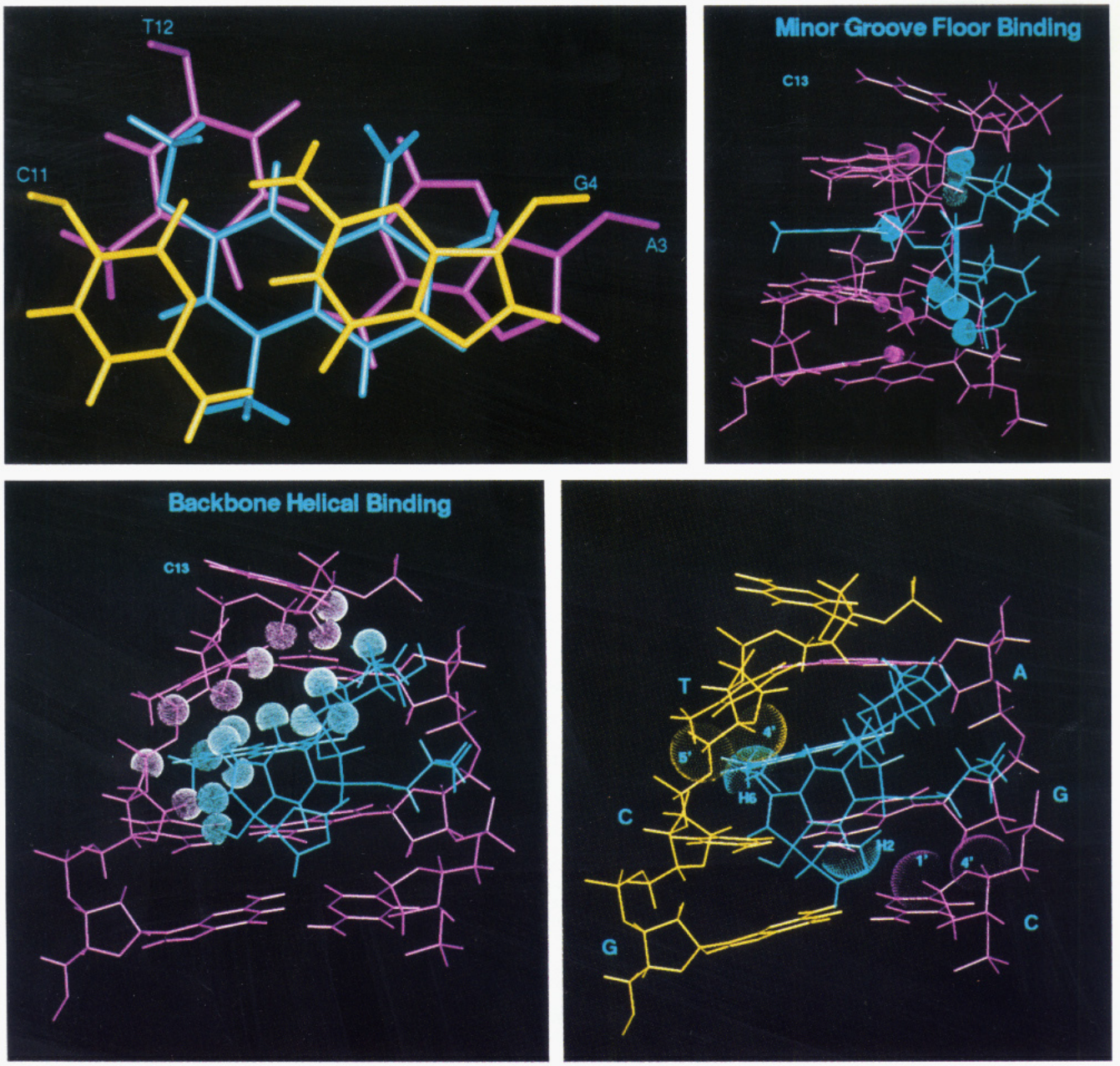

FIGURE 6: Intermolecular interactions and the cleavage site in the complex. DNA strands are colored in magenta/yellow and NCSi-glu is in light blue. (A, top left) Stacking at the intercalation site viewed down from the G4•C11 end with the NPH ring of NCSi-glu shown in light blue. (B, bottom left) Backbone helical binding interfaces viewed into the minor groove along the G10C11T12C13 strand. Van der Waals radii of hydrogen were drawn at 50% of full scale, illustrating the complementary surfaces between the helical backbone of the DNA duplex and NCSi-glu. (C, top, right) Side view of the binding interfaces involving NCSi-glu and DNA base substituent groups on the minor groove floor. Van der Waals radii were drawn at 50% of full scale for the hydrogens located at the floor of the minor groove. The G4 and G10 amino groups in the minor groove are distinguished by further reduced van der Waals radii. (D, bottom right) Geometry at the AGC•GCT lesion sites shown by 100% van der Waals radius drawing. The NCSi-glu(H6) is proximal to the T12(H4′) and T12(*pro-S* H5′), while NCSi-glu(H2) is at a moderate distance to the C5(H1′) and C5(H4′).

NCSi-glu between the 5′-CT/5′-AG step presents a unique binding mode, since most intercalation ligands prefer alternating purine−pyrimidine GC/GC sites (actinomycin, daunomycin, echinomycin), AT/AT sites (CysMe-TANDEM), and AC/GT sites (nogalamycin and luzopeptin) (Neidle & Abraham, 1984; Wang et al., 1984; Gao & Patel, 1989; Zhang & Patel, 1990, 1991; Addess et al., 1992; Waterloh et al., 1992). Molecular interactions at the interfaces of the pyrimidine−pyrimidine/purine−purine CT/AG intercalation site in the NCSi-glu−DNA complex should expand our views on DNA recognition by the intercalating ligands.

The most distinctive feature of the backbone helical contact interface is the formation by NCSi-glu of a right-handed hydrophobic surface, which is complementary to the curvature of the right-handed DNA helix (Figure 6B). This alignment of the complex is stabilized by many van der Waals interactions (Table 2), which involve the helical sugar−phosphate backbone of the C11T12C13 segment of the duplex on one side and the NMF sugar, the hydrophobic edge of THI, and the 7″-methoxy group of NPH on the other side. The orientation of the NMF sugar permits the maximum utilization of lipophilic hydrogens in its interactions with the deoxyribose moieties and the hydrogen bond formation between NCSi-glu(HO3′ and HO4′) and DNA C13(O3′ and 5′-phosphate oxygen), respectively (Figure 6B). Formation of nonexplicit hydrogen bonds between the NMF

of NCSi-glu and DNA phosphates was previously postulated in a modeling study (Elbaum & Schreiber, 1994).

There are fewer interactions between NCSi-glu and the backbone of the A3 strand (Table 2). Interestingly, the hydrogen of the 2″-OH group of NCSi-glu protrudes from the NPH ring plane, making van der Waals contacts with H1′, H2′, and H2″ of the A3 sugar (Figure 6B, Table 2). There is no indication of electrostatic interactions involving the naphthoate 2″-hydroxyl. A set of contacts between NCSi-glu and the minor groove floor were detected, which include interactions of NPH(H8″) and THI (H2, H11, *pro*-S H14) of NCSi-glu with DNA A3(H2) and the amino protons of G4 and G10 (Figure 6C, Table 2). It is important to point out that DNA protons contributing to these intermolecular contacts bear the signature of the individual bases, and thus, the minor groove contacts are critical for the sequence specificity of complex formation (*vide infra*). There is no indication of intermolecular hydrogen bonds involving G4 and G10 amino protons, in contrast to many examples of such hydrogen bonds found in a number of ligand−DNA complexes (Gao & Patel, 1989).

Conformation of DNA. Table S2 lists parameters which describe the distinctive DNA conformation in the NCSi-glu−DNA complex. The binding of NCSi-glu to the duplex induces large structural distortions at the binding site (Figure 5). This is characterized by a significant increase in base rise, which is 8.2 ± 0.1 Å base−base separation at the intercalation site, the large and opposite buckle angles, which are 24.5 ± 1.9° and −26.5 ± 1.8° for A3•T12 and G4•C11 base pairs, respectively, and a total of 23.5° unwinding (based on the averaged structure) in the trinucleotide G2A3G4•C11T12C13 sequence. The C11−T12 linkage is more extended than the A3−G4 linkage of the opposite strand due to the spatial requirement of the methyl groups of NPH (Figure 5). DNA base moieties on either side of the NPH ring exhibit a large tilt to minimize the gap created by NPH intercalation, resulting in a unique V-shaped intercalation site (Figure 5A). The unwinding of the helix in the NCSi-glu−DNA complex mostly occurs at the A3•T12/G4•C11 step (Table S2). This result is consistent with the downfield-shifted A3/G4 and C11/T12 ^{31}P resonances at −2.06 and −3.36 ppm, respectively. In contrast, other ^{31}P resonances of the duplex were clustered in the −3.6 to −4.3 ppm spectral region (Table 1). The degree of total unwinding is in good agreement with the reported experimental value of 21° in native NCS chrom−DNA complexes (Povirk et al., 1981). Measurements of the major and minor grooves of the duplex indicate that both grooves become wider and shallower at the binding region (A3G4C5• G10C11T12) (Figure 5B) compared to the free DNA duplex.

Structural Correlations of NCS Chrom Sequence Specificity. NCSi-glu is a structural isoform of the activated 2,6-biradical species of NCS chrom (Figure 1). Inspection of the NCSi-glu−DNA complex structure reveals several specific interactions which correlate well with the base specificity of ss and sequence specificity of ds lesions induced by the NCS chrom. One set of interactions involves protons of NMF and THI of NCSi-glu and A3(H2) of the DNA (Table 2). The *N*-methyl group is directed toward C13 in the 3′-direction of the T12 strand and is in close contact with A3(H2) (Figures 1 and 3B). This specific recognition of the adenine base by the carbohydrate unit may explain the affinity of NCS chrom for the T•A-rich sequences and the high frequency of ss cleavage at T residues. This assessment is consistent with the marked increase in ss cleavage at C paired with an inosine, which is similar to adenine in containing a base H2 proton, instead of a G (Lee et al., 1989). The proposed hydrogen bonding between the protonated N2-methyl of the NCS thiol adducts and the T(O2) by modeling (Sugiyama et al., 1992) is nonexistent in the NMR-derived structure.

The sequence specificity of ds damage may be related to two sets of interactions, which correlate H2 and H12 of NCSi-glu with the G4 minor groove protons (H1′ and amino protons) of the DNA and H2, H14 cyclocarbonate methylene protons and HO4 of NCSi-glu with the G10 amino group of the DNA. A key piece of experimental evidence is the NOE between G4(H1′) and NCSi-glu(H12) (Table 2), while G amino protons were not observed in 2D NMR spectra recorded in H_2O. The structure of NCSi-glu shows that the H2, H12, and HO4 of NCSi-glu form a groove floor binding interface, which recognizes the amino groups of G4 and G10, respectively (Figure 6C). Therefore, the positioning of these amino groups of the G residues adjacent to the T•A sites provides a molecular basis for the specific ds cleavage of the target DNA sequence. This minor groove interface modulation can be further illustrated by two interesting experimental observations. In oligonucleotides containing an AGC•gcT site, when the amino group of G was replaced by a hydrogen by a guanine to inosine (I) substitution, abasic site formation decreased. On the other hand, when the amino group of g was replaced by an I, a 4-fold enhancement of abasic site formation was observed (Kappen et al., 1988). The available structure permits further structure determinations/modeling experiments, which are to discern detailed interactions at the groove binding interface in various NCS chrom−DNA complexes containing ANN•N′N′T trinucleotide binding sites (N and N′ can be Watson−Crick base pairs or mismatches) (Goldberg, 1991; Lam et al., 1991; Sugiyama et al., 1992).

The lifetime of the semireduced biradical species of NCS chrom is expected to be extremely short; thus ds cleavage is most likely to occur only when the 2,6-biradical THI is favorably positioned at the vicinity of double-strand target sites. This would permit concerted T(H5′) and C(H1′) abstraction by the radicals at the C6 and C2 positions, respectively. The structure of the complex (Figure 6D) shows that NCSi-glu(H6) is proximal to T12(*pro-S* H5′) (2.87 ± 0.02 Å) and to T12(H4′) (2.14 ± 0.01 Å). Predominant H5′ abstraction in DNA strand cleavage reactions may be explained by the rotational flexibility of the C5′ bonds to position H5′ in a favorable orientation and distance to the 6-position of the activated NCS chrom. The NCSi-glu(H2) and the C5(H1′) site are moderately separated by 3.78 ± 0.09 Å. This is consistent with the lower frequency of H1′ abstraction by the C2 radical and ease of C2-radical quenching by solvent or adducted thiol (Wender & Tebbe, 1991; Chin & Goldberg, 1993).

CONCLUSION

The postactivated NCSi-glu−DNA structure provides primary answers to the sequence specificity of NCS chrom binding and cleavage of the target DNA duplexes. The structure predicts that the binding specificity of NCS chrom is determined by the 2′-*N*-methyl sugar moiety, which

recognizes the T•A base pair and assists the positioning of the NPH ring between T•A and the adjacent C•G base pair in the 5′-direction from T. Guided by the orientation of these substituent groups, the enediyne ring snugly fits into the minor groove in an orientation which is governed by the specific interactions with the functional groups featuring the DNA minor groove floor. The interplay of the molecular forces and the surface fit of the two parties result in sequence-specific H-abstraction and strand cleavage of the target DNA sequences. The revelation of these intermolecular contacts reveals the critical role played by the G amino groups in stabilizing NCS chrom binding to double-stranded DNA. The DNA duplex possesses distinct structural features in the complex which are characterized by an extended, unwound V-shaped intercalation site and wider and shallower grooves. The reported structures provide a basis for modeling various NCS chrom−DNA complexes which contain sequence-specific lesion sites and designing NCS chrom analogs of improved chemical and biomedical properties.

ACKNOWLEDGMENT

The 600-MHz NMR spectrometer at the University of Houston was funded in part by the W. M. Keck Foundation. The authors are grateful for the 750-MHz NMR instrument time provided by Bruker Analytische Messtechnik GMBH (Germany) and the considerable assistance by Ralf Ruin in using the Bruker NMR facility. The CURVES program is a gift from Dr. Lavery. X.G. and J.S.R. thank Dr. Ji Jie for providing programs for semiautomated NOE assignments and preparation of distance restraint files and Dr. Juan Gu for processing some of the NMR data. A.S. and I.H.G. wish to thank Dr. G. Kellog for assistance with the computer visualization of the complexes and Dr. C. Walsh for use of his computer equipment.

SUPPLEMENTARY MATERIAL AVAILABLE

Two tables giving proton assignments of the free DNA duplex and chemical shift differences between the duplex in the NCSi-glu−DNA complex and the free DNA duplex and structure parameters of the DNA duplex in the NCSi-glu−DNA complex (3 pages). Ordering information is given on any current masthead page.

REFERENCES

Addess, K. J., Gilbert, D. E., Olsen, R., & Feigon, J. (1992) *Biochemistry 31*, 339.

Chin, D.-H., & Goldberg, I. H. (1993) *Biochemistry 32*, 3611.

Dasgupta, D., & Goldberg, I. H. (1985) *Biochemistry 24*, 6913.

Dedon, P. C., & Goldberg, I. H. (1992) in *Nucleic Acid Targeted Drug Design* (Probst, C., & Perun, T., Eds.) p 475, Marcel Dekker, New York.

Dedon, P. C., Jiang, Z.-W., & Goldberg, I. H. (1992) *Biochemistry 31*, 1917.

Edo, K., Mizugaki, M., Koide, Y., Seto, H., Furihata, K., Otake, N., & Ishida, N. (1985) *Tetrahedron Lett. 26*, 331.

Elbaum, E., & Schreiber, S. (1994) *Bioorg. Med. Chem. 4*, 309.

Galat, A., & Goldberg, I. H. (1990) *Nucleic Acids Res. 18*, 2093.

Gao, X., & Jones, R. A. (1987) *J. Am. Chem. Soc. 109*, 1275.

Gao, X., & Patel, D. J. (1989) *Q. Rev. Biophys. 22*, 93.

Gao, X., & Burkhart, W. (1991) *Biochemistry 30*, 7730.

Goldberg, I. H. (1991) *Acc. Chem. Res. 24*, 191.

Golik, J., Clardy, J., Dubay, G., Groenewold, G., Kawaguchi, H., Konishi, M., Krishnan, B., Okhuma, H., Saitoh, K., & Doyle, T. W. (1987) *J. Am. Chem. Soc. 109*, 3461.

Hawley, R. C., Kiessling, L. L., & Schreiber, S. L. (1989) *Proc. Natl. Acad. Sci. U.S.A. 86*, 1105.

Hensens, O. D., Chin, D.-H., Stassinopoulos, A., Zinc, D. L., Kappen, L. S., & Goldberg, I. H. (1994) *Proc. Natl. Acad. Sci. U.S.A. 91*, 4534.

Ishida, N., Miyazaki, K., Kumagai, K., & Rikimaru, M. (1965) *J. Antibiot. Ser. A 18*, 68.

Kappen, L. S., & Goldberg, I. H. (1993) *Science 261*, 1319.

Kappen, L. S., Chen, C., & Goldberg, I. H. (1988) *Biochemistry 27*, 4331.

Kim, K.-H., Kwon, B.-M., Myers, A. G., Rees, D. C. (1993) *Science 262*, 1042.

Konishi, M., Okhuma, H., Tsuno, T., Oki, T., VanDune, G. D., & Clardy, J. (1990) *J. Am. Chem. Soc. 112*, 3715.

Kaszewski, J. K., Nilges, M., & Brünger, A. T. (1992) *J. Biol. NMR 2*, 33.

Lam, K. S., Hesler, G. A., Gustavson, D. R., Crosswell, A. R., Veitch, J. M., & Forenza, S. (1991) *J. Antibiot. 44*, 472.

Langley, D. R., Golik, J., Krishnan, B., Doyle, T. W., & Beveridge, D. L. (1994) *J. Am. Chem. Soc. 116*, 15.

Lavery, R., & Sklenar, H. (1988) *J. Biomol. Struct. Dyn. 6*, 63.

Lee, M. D., Dunne, T. S., Siegel, M. M., Chang, C. C., Morton, G. O., & Borders, D. B. (1987) *J. Am. Chem. Soc. 109*, 3464.

Lee, S. H., Thivierge, J. O., & Goldberg, I. H. (1989) *Nucleic Acids Res. 17*, 5809.

Meschwitz, S. M., & Goldberg, I. H. (1991) *Proc. Natl. Acad. Sci. U.S.A. 88*, 3047.

Meschwitz, S. M., Schultz, R. G., Ashley, G. W., & Goldberg, I. H. (1992) *Biochemistry 31*, 9117.

Myers, A. G. (1987) *Tetrahedron Lett. 28*, 4493.

Napier, M. A., Holmquist, B., Strydom, D. J., & Goldberg, I. H. (1979) *Biochem. Biophys. Res. Commun. 89*, 635.

Neidle, S., & Abraham, Z. (1984) *Crit. Rev. Biochem. 17*, 73.

Nicolaou, K. C., & Dai, W.-M. (1991) *Angew. Chem., Int. Ed. Engl. 30*, 1387.

Otani, T., Minami, Y., Marunaka, T., Zhang, R., & Xie, M.-Y. (1988) *J. Antibiot. 41*, 1580.

Paloma, L. G., Smith, J. A., Chazin, W. J., & Nicolaou, K. C. (1994) *J. Am. Chem. Soc. 116*, 3697.

Planteau, P., & Guéron, M. (1982) *J. Am. Chem. Soc. 104*, 7301.

Povirk, L. F., & Goldberg, I. H. (1980) *Biochemistry 19*, 4773.

Povirk, L. F., & Goldberg, I. H. (1985) *Proc. Natl. Acad. Sci. U.S.A. 82*, 3182.

Povirk, L. F., Dattagupta, N., Warf, B. C., & Goldberg, I. H. (1981) *Biochemistry 20*, 4007.

Quigley, G. J., Wang, H.-J., Ughetto, G., van der Marel, G. A., van Boom, J. H., & Rich, A. (1980) *Proc. Natl. Acad. Sci. U.S.A. 77*, 7204.

Sugiyama, H., Fujiwara, T., Kawabata, H., Yoda, N., Hirayama, N., & Sato, I. (1992) *J. Am. Chem. Soc. 114*, 5573.

Walker, S., Murnick, J., & Kahne, D. (1993) *J. Am. Chem. Soc. 115*, 7954.

Wang, H.-J., Ughetto, G., Quigley, G. J., Hakoshima, T., van der Marel, G. A., van Boom, J. H., & Rich, A. (1984) *Science 225*, 1115.

Waterloh, K., Olsen, R. K., & Fox, K. R. (1992) *Biochemistry 31*, 6246.

Wender, P. A., & Tebbe, M. J. (1991) *Tetrahedron Lett. 32*, 4863.

Wuthrich, K. (1986) *NMR of Proteins and Nucleic Acids*, John Wiley & Sons, New York.

Zhang, X., & Patel, D. J. (1990) *Biochemistry 29*, 9451.

Zhang, X., & Patel, D. J. (1991) *Biochemistry 30*, 4026.

BI942100L